Scientific Research Publishing

Open Journal of Geology, 2024, 14, 989-1015
https://www.scirp.org/journal/ojg
ISSN Online: 2161-7589
ISSN Print: 2161-7570

Hydrothermal Alteration Associated with the Kiaka World-Class Gold Deposit (Burkina Faso, West Africa)

Benjamin Sawadogo[1,2*], Gounwendmanaghré Hubert Zongo[1,3], Wilédio Marc-Emile Bonzi[2,4], Kalidou Traore[5], Sâga Sawadogo[1], Ousseni Yameogo[6], Ousmane Bamba[1], Guy Franceschi[7]

[1]Laboratoire Géosciences & Environnement (LaGE), Département des Sciences de la Terre, Université Joseph Ki-Zerbo, Ouagadougou, Burkina Faso
[2]IRD, Ouagadougou, Burkina Faso
[3]Ecole Supérieure d'Ingénieries, Université de Fada N'gourma, Fada N'Gourma, Burkina Faso
[4]Unité de Formation et de Recherche en Sciences Appliquées et Technologies (UFR-SAT), Université Daniel Ouezzin Coulibaly, Dédougou, Burkina Faso
[5]Laboratoire de Géodynamique et de Cartographie, des Techniques et des Technologies de Bamako, Université des Sciences, Bamako, Mali
[6]West African Resources LTD, Ouagadougou, Burkina Faso
[7]GF Consult bvba, Gent, Belgium
Email: *sawadogobenja@gmail.com

How to cite this paper: Sawadogo, B., Zongo, G.H., Bonzi, W.M.-E., Traore, K., Sawadogo, S., Yameogo, O., Bamba, O. and Franceschi, G. (2024) Hydrothermal Alteration Associated with the Kiaka World-Class Gold Deposit (Burkina Faso, West Africa). *Open Journal of Geology*, **14**, 989-1015.
https://doi.org/10.4236/ojg.2024.1412044

Received: October 5, 2024
Accepted: December 3, 2024
Published: December 6, 2024

Abstract

This paper aims to show the relationships between hydrothermal alteration, deformation and gold mineralization in the main area of the Kiaka deposit. The Kiaka gold deposit is located in the South-central of Burkina Faso in the Tenkodogo volcano-sedimentary belt. Mineralization is primarily hosted by amphibolite, mylonitized quartz microdiorite and meta-sediment. The combination of petrographic, metallographic and geochemical analysis along with structural deformation of the ore body allowed us to distinguish the three main stages of hydrothermal alteration in the Kiaka gold deposit. (i) The first stage is characterized by ductile deformation which induces potassic- and LILE-rich alteration with crystallization of disseminated pyrrhotite. (ii) The second stage corresponds to chloritization and is associated with a brittle-ductile deformation and retrograde metamorphism. A second generation of disseminated pyrrhotite and a few pyrite and chalcopyrite crystallized during this event. Pyrrhotite also fills veins. (iii) The third alteration stage is characterized by a significant carbonation and concurrent with a brittle deformation. It is accompanied locally by a high-grade gold mineralization (up to 29 g/t).

Keywords

Gold Deposit, Hydrothermal Alteration, Deformation, Geochemistry,

Burkina Faso

1. Introduction

Gold indices or deposits in Burkina Faso, similarly to those in many West African countries, are located in volcano-sedimentary birimian belts [1] that underwent a low-grade regional metamorphism [2] [3]. It has long been considered that gold mineralization occurs in Burkina Faso as dissemination in hydrothermally altered volcano-sedimentary units, albitite and listvenite, and also as quartz veins associated to sulfides and tourmaline [2] [4] [5]. The genesis of these deposits might be synchronous with regional tectono-metamorphic-thermal events accompanied by the circulation of hydrothermal fluids [2] [5] [6]. Hydrothermal fluids play a leading role in the genesis of primary gold mineralization. Indeed, the metallic deposits that occur in the upper part of the lithosphere are genetically linked with hydrothermalism, except those who derive from magmatic processes [7]. Those deposits are created by the percolation of hydrothermal brines that extracted metals from a source rock, transported them as ionic complexes and precipitate them in a favorable set-up [7] [8]. The fluids are channeled by the permeability of country rocks, which is enhanced by tectonic deformational structures [9]-[11]. The interaction of the migrating fluid with country rock induces reactions resulting in a metasomatism or a chemical disequilibrium of the country rock. The chemical exchanges between hydrothermal fluids and wall rocks are characterized by a modification of the chemistry and the mineralogy termed as a hydrothermal alteration [8]. In the case of the Kiaka, a world-class deposit located in the center-south of Burkina Faso (**Figure 1**), successive hydrothermal alterations are related with the long-lasting gold mineralization (2140 - 2100 Ma) and the structural evolution of the district, from early birimian age [12]. The deposit exhibits a potassic alteration style, such as biotitization that is observed in some west-African gold deposits [13], and is barely described in birimian fields in Burkina Faso [12]. The highlight of hydrothermal alterations of the Kiaka deposit could bring a fundamental understanding of the onset of hydrothermal alteration over the eburnean orogeny, and understand the processes involved in gold mineralization in volcanosedimentary belts.

In this paper, we describe and identify mineralogic evolution of hydrothermal alteration in Kiaka gold deposit with a systematic sequence of alterations, adding a perspective from whole rock geochemistry.

2. Study Area and Geological Context

2.1. Regional Geological Setting

The geological foundation of Burkina Faso is largely dominated by a Paleoproterozoic granite-greenstone terrain also known as Birimian crust (2.27 - 1.96 Ga) [14] [15]. It is exposed to the NE of the Baoulé-Mossi domain which is the eastern part of the

sWAC (**Figure 1**). The Birimian crust of the Baoulé-Mossi has a geochemical juvenile signature [15]-[22] and shows an organization of lithological sequences. Thus, the greenstones are composed of metamorphosed bimodal tholeiitic to calc-alkaline volcanic, volcano-sedimentary and sedimentary rocks [23]-[26]. Bulk birimian greenstone belts lithologies are dominated by basalt/andesite, gabbro/dolerite with intercalations of metasediments and/or carbonaceous beds, volcanoclastites, turbidites, graphitic sediments interlaid with calc-alkaline volcanic rocks [24] [27]. They are intruded or bordered firstly by several calc-alkaline to alkaline generations of TTG-type granitoids and secondly by granitic to leucogranitic plutons [18] [19] [25] [28]-[32]. Most of the granitoids are composed of gneiss, amphibole bearing intermediary to felsic granitoids, biotite granitoids and late K-rich granite units [23] [33]-[35]. They occupy the larger surface of the Baoulé-Mossi domain (**Figure 1**). Many studies highlighted the relationship between these granitoids as successive generations of syn to late tectonic intrusions [18] [19] [23] [25] [29] [36]-[39] or products of partial melting of birimian first or older units [18] [40]. Late coarse-grained sedimentary rocks form the so called Tarkwaian units [41]-[43] deposited on top of the former rocks. Their late age of formation is important in exploration.

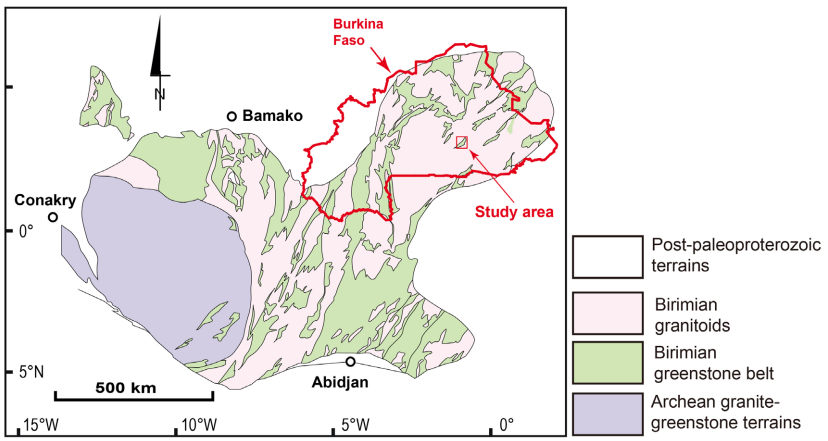

Figure 1. Location of the Kiaka gold deposit in the southern west African craton (modified after [45]).

The Birimian crust has been accreted and deformed during the eburnean tectono-thermal orogenesis which ended towards 2 Ga [14] [23] [44] and resulted in the formation of many regional to local shear zones [44] [45]. Deformation derives from the collision between the Baoulé-Mossi domain in accretion with the more rigid Archean Kenema-Man domain exposed to the western part of the Baoulé-Mossi domain [44] [46]. It has driven to a wide range of recorded metamorphic conditions in the Birimian crust of the Baoulé-Mossi domain as highlighted in many studies. So, regional greenschist facies are the most pervasive metamorphic condition interpreted coeval with the main eburnean deformation [18] [22] [27] [47]-[51]. The amphibolite facies are detected surrounding the contact zones

between volcanosedimentary rocks and some granitoids domains, suggesting a contact metamorphism for their genesis [19] [29] [52] [53]. A high pressure—low to middle temperature metamorphic rocks are identified and mapped in juxtaposition with low grade metamorphic rocks in Ghana [54]-[56] and in eastern Burkina Faso [57]. They are interpreted as lower Birimian crust kinematically exhumed during transpressionnal partitioned regional eburnean deformation [44] [54] [55].

The long-lived evolution of the eburnean accretion/collision orogen of the Baoulé-Mossi, the juvenile character of the crust, his lithological diversity and his high shear zones density [44] [45] are critical features to explain hydrothermal fluids path, channeling, interaction with rocks, alteration, ore deposits and mineralization genesis [1] [3] [28] [58]-[60]. These thus explain why hydrothermal activity and alteration are associated to all deposits in the sWAC (cf synthesis of [60] and constitute key features to focus on when prospecting). But it exists a wide range of hydrothermal alteration facies, depending specifically on host rocks types. In the following, we are showing the features of hydrothermal alteration related to Kiaka Gold deposit.

2.2. Local Geological and Structural Setting

The Kiaka gold deposit is located 140 km southeast of Ouagadougou, in the Tenkodogo district (Center-South, **Figure 1**). The deposit is hosted by a greenstone belt composed of quartz-biotite metagreywacke, aluminosilicate-bearing metapelite, garnet-orthopyroxene-bearing schist and volcanic units [12]. This belt is associated with a foliated biotite-amphibole diorite dated at 2140 ± 8 Ma by U-Pb on zircon [12]. This diorite is among the regional tonalite-trondhjemite-granodiorite (TTG)-like granitoids [29] [33] which are among the oldest plutonic rocks of the Baoulé-Mossi domain [14] [30] [31]. That means that the country rocks of the Kiaka gold deposit lasted long evolution and preservation, classifying the mineralization among the first gold deposits of the craton [60].

Regional eburnean deformation is expressed locally by NE-SW ductile and brittle structures due to an initial rheological contrast of the rocks, crosscut by the late-orogenic Tiebele-Dori-Markoye corridor (**Figure 2**). In volcano-sedimentary units, the present structures are a S_0 stratification accompanied by a slaty cleavage developed conformably with the regional NE-SW trend [28]. In granitoids, deformation is expressed by banding, magmatic foliation and mineral lineation. In the study area, the ductile deformation occurs associated with NE-SW-trending mylonitic shear zones [33]. The brittle deformation is characterized by fracture opening, veins and frequent quartz, pegmatite and aplite dykes also oriented in the NE-SW regional trend [33]. All the former structures show a crosscutting relationship pattern with dolerite dykes oriented along a NW-SE direction. These dykes may be interpreted as late to post-eburnean brittle events [33] [61] [62].

The NE-SW structural grain of the study area is typical of all the southern and the eastern part of Burkina Faso [29] [33] [63]-[69]. This structural pattern

adopted by tectonic fabrics which are steeply dipping and by transcurrent shear zones associated with reverse movements is coupled with local folds and lineations with variable dip but dominated by high values [12]. This suggests intense deformation and transpression as the main deformation mode [44] [45]. However, the overall NE-SW orientation argues for a general NW-SE shortening.

The Kiaka Gold deposit appears as NE-SW subparallel elongated ore bodies, mainly hosted within shear zones and in apparent axial plane of folds [12]. This indicates an orogenic gold type mineralization. Two styles of mineralization have been identified with different hydrothermal alteration, widely explained in this paper. The disseminated gold style with mineralization scattered parallel to regional orientation, occurred during the first mineralization event, constrained by 2157 ± 24 Ma Re-Os age on pyrrhotite [12] [60]. This event is contemporaneous with local shear zones activity constrained by the 2140 ± 7 Ma U-Pb on zircon age of the sheared dioritic intrusion [12]. This is in agreement with structural control of the deposit and also gives evidence that this first event lasted until after 2140 ± 7 Ma. The veining/veinlet gold style mineralization event comes after, suggesting the change in local rocks behavior (from ductile to ductile-brittle or simply brittle) during the ongoing regional progressive deformation. Therefore, the Kiaka Gold deposit forms a vast low-grade system with measured and indicated resources of 124 Mt at 1.09 g/t Au (3.9 Moz) and inferred resources of 27 Mt at 0.83 g/t Au (0.8 Moz) [12]. The formation of that system occurred following a retrograde metamorphic evolution from lower amphibolite facies during the first mineralization event to upper greenschist facies conditions during the second one.

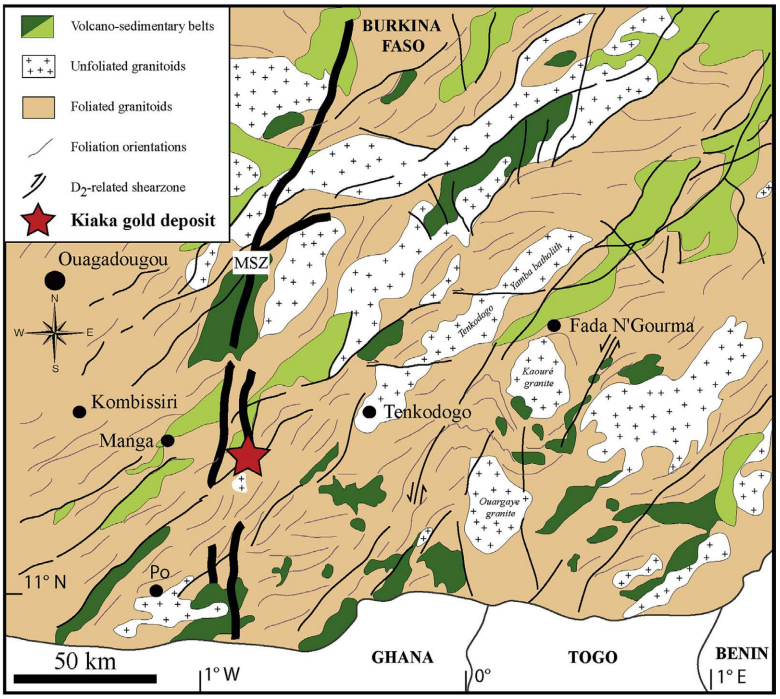

Figure 2. Local geology of the study area (After [12]; Tiebele-Dori-Markoye corridor represented by the thick black line).

3. Methodology

3.1. Sampling

The work was carried out in two phases: fieldwork in the Kiaka deposit and petrographic, metallographic characterization in the Laboratory Géosciences et Environnement of the Joseph Ki-Zerbo University (Ouagadougou, Burkina Faso).

The fieldworks involved the identification of a suitable drilling which crosses the mineralized zone with a good representativity of the roof and bottom host rocks, and exposes the potential of the deposit. The selected drill hole was the drill KDH258 (Figure 3), that crosses the mineralized zone, and in which a relatively high gold content was recorded (29 g/t). In addition to this drilling, six supplementary drillings located along the structure, and that also crosscut the mineralized zone, were chosen for the study. Each drilling was sampled in the mineralized zone and in the distal barren surrounding rocks. Concerning the KDH258 survey centered on the deposit, we sampled systematically all the holes from the upper distal zone to the lower distal zone, the hanging walls and the mineralized body (Figure 3).

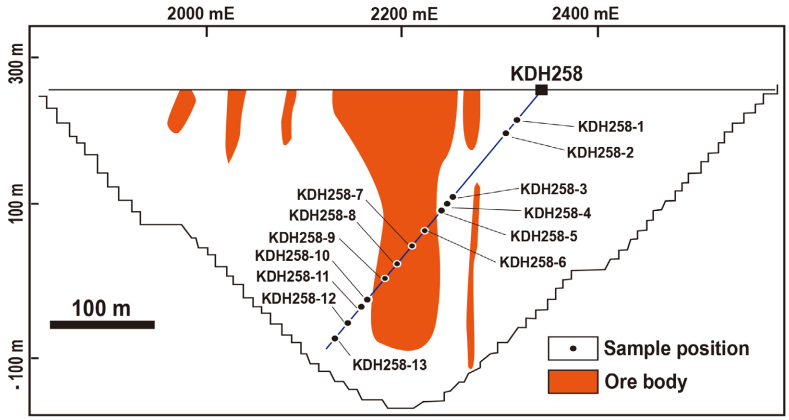

Figure 3. Exploration section illustrating the core of the Kiaka deposit, intersected by the KDH258 drill hole, which was systematically sampled from top to bottom (refers to Table 1 for the ICP-MS geochemical analysis results of the samples).

3.2. Microscopic Observations

The samples collected on the 7 drillings were prepared for the conception of polished thin sections in the Laboratoire Géosciences et Environnement (LaGE). The microscopic observations were realized with a polarizing microscope in natural transmitted and reflected light. The microscopic studies were carried out using a polarizing microscope in transmitted and reflected light, with the following objectives:

(i) petrographic characterization,

(ii) identification of alteration-related minerals and paragenesis,

(iii) characterization of hydrothermal alteration-related metals associations,

(iv) the characterization of metal suites related to hydrothermal alteration.

3.3. Geochemistry

Geochemical analyses were realized to characterize the geochemical processes linked to fluid circulation in the Kiaka deposit. The samples were taken from the KDH258 drill hole. The selection of the samples is divided as follows: 4 samples from the distal zone (top and bottom on the mineralized zone), 4 samples in the top and floor walls of the mineralization, and 4 samples in the mineralized body.

The samples were crushed and analyzed by Activation Laboratories Ltd. (Actlabs) in Canada. The samples were prepared by fusion with lithium tetraborate and lithium metaborate. Major elements, Sc, Be, V, Ba, Sr, Y and Z were analyzed by inductively coupled plasma atomic emission spectrometry (FUS-ICP). The other trace elements Cr, Co, Ni, Cu, Zn, Ga, Ge, As, Rb, Nb, Mo, Ag, In, Sn, Sb, Cs, rare earth elements, Hf, Ta, W, Tl, Pb, Bi, Th and U were analyzed by mass spectrometry (FUS-MS). The details of the analysis procedure are available on the Actlabs website (https://actlabs.com/geochemistry/lithogeochemistry-and-whole-rock-analysis/). The Au content in all the selected boreholes was provided by the company (B2GOLD) operating on the Kiaka deposit. These results originate from a fire assay of duplicate samples.

4. Results

4.1. Petrographic Observations

The geological setting of the mineralized zone is characterized by three lithologic units that are metasediments, amphibolite, and mylonitized quartz microdiorite.

4.1.1. Metasediments

The metasedimentary formations of the study area appear with a grey to often dark coloration, and are diversely affected by the deformation. They have a granolepidoblastic texture composed of quartz (50% - 60%) with rare relicts of potassic feldspar, and phylliteous minerals (biotite and white mica flakes, 40%) that underline a slaty cleavage that we assimilate to a D1 deformation. (**Figure 4**).

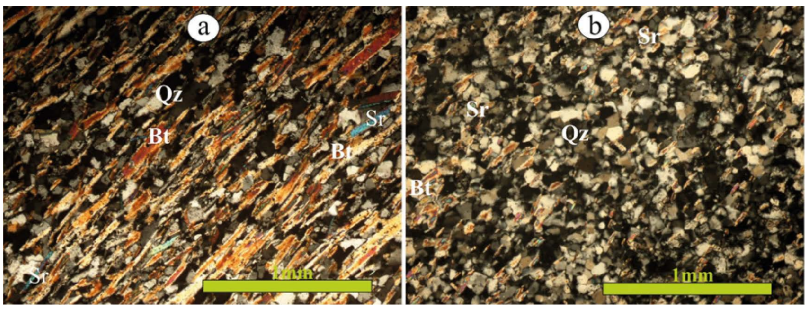

Figure 4. Photomicrographs of sedimentary rocks (cross-polarized light). (a) Mica-rich metasediment. (b) Mica-poor metasediment. Abbreviations: Bt = biotite, Qz = quartz, Sr = sericite.

4.1.2. Amphibolite

They are greenish to dark-colored rocks with fine-grained sizes composed of 80% of dark minerals and 20% of light minerals (**Figure 5(a)**). At a microscopic scale,

their texture ranges from nematoblastic to fine-grained porphyroidic. The mineralogical composition is dominated by green hornblende (70%) that is often destabilized in fibrous actinote or in carbonate (Figure 5(b)). Plagioclase (10%) is subhedral to euhedral and sometimes shows an alteration to white mica or carbonate. Quartz (5% - 10%) is seen as undulating subgrains that suggest its secondary character. Amphibolite also contains accessory garnet and relicts of pyroxenes.

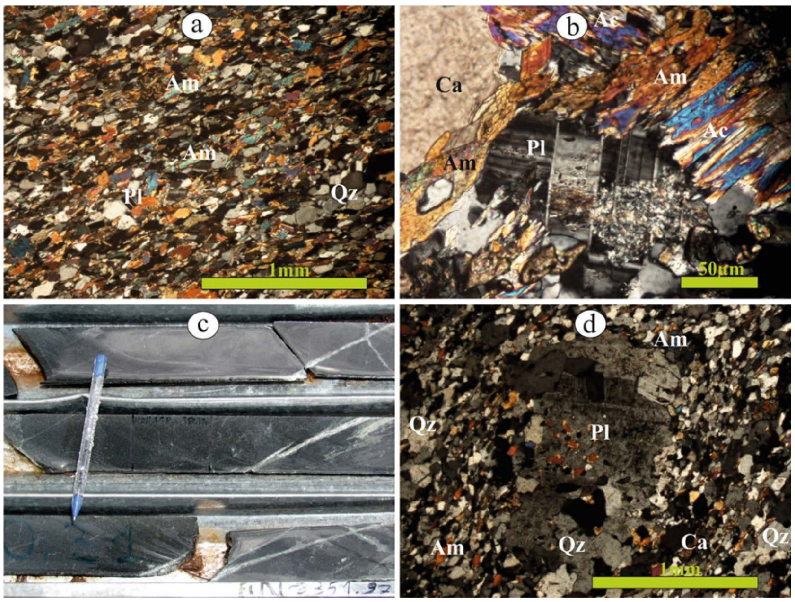

Figure 5. Photomicrographs of basic and acid intrusive rocks (cross-polarized light, corresponds to the sample KDH258-1, see position in Figure 3). (a) Amphibolite wrapped by a soft slate cleavage. (b) Destabilization of hornblende to fibrous actinote, and replacement of quartz to carbonate. (c) Macroscopic view of a meta-quartz microdiorite. (d) Phenocryst of poikilitic plagioclase with quartz inclusion, and amphibole forming an asymmetric pressure shadow. Abbreviations: Am = Amphibole, Ac = Actinote, Ca = carbonate, Pl = plagioclase, Qz = quartz.

4.1.3. Mylonitized Quartz Microdiorite

The fine-grained recrystallized and locally porphyritic facies with plagioclase phenocrysts appear with a greenish-gray color (Figure 5(c)). They contain porphyroclasts (about 15 - 20%) composed of plagioclase, poikilitic amphibole and rarely quartz. The quartz porphyroclasts undergo a subgrain recrystallization that results in a microcrystalline matrix. Except for the quartz, the microlithic matrix is composed of plagioclase, amphibole and biotite flakes (Figure 5(d)). Accessory minerals are oxides, iron-hydroxides and opaque minerals.

4.2. Hydrothermal Alteration and Mineral Paragenesis

The mineralogical analysis of the mineralized zone exhibits three types of hydrothermal alteration related to the Kiaka gold deposit. In chronological order, we have potassic alteration, chloritization and carbonation.

4.2.1. Potassic Alteration

This alteration is characterized in amphibolite by a biotitization distinguished by

the brown coloration of dark micas in hand samples. Biotite forms clusters arranged parallel to the cleavage planes (Figure 6(a)). The microscopic observation reveals that biotitization consists of a destabilization of hornblende in fine biotite flakes (Figure 6(b)) or in biotite + epidote (Figure 6(c)). The potassic alteration is also highlighted by the transformation of plagioclases into white micas and rarely microcline. It is also associated with the crystallization of tourmaline and the formation of iron-titanium-oxides. Tourmaline is generally disposed along the cleavage planes created by biotitized amphibole layers. This alteration is accompanied by the crystallization of pyrrhotite.

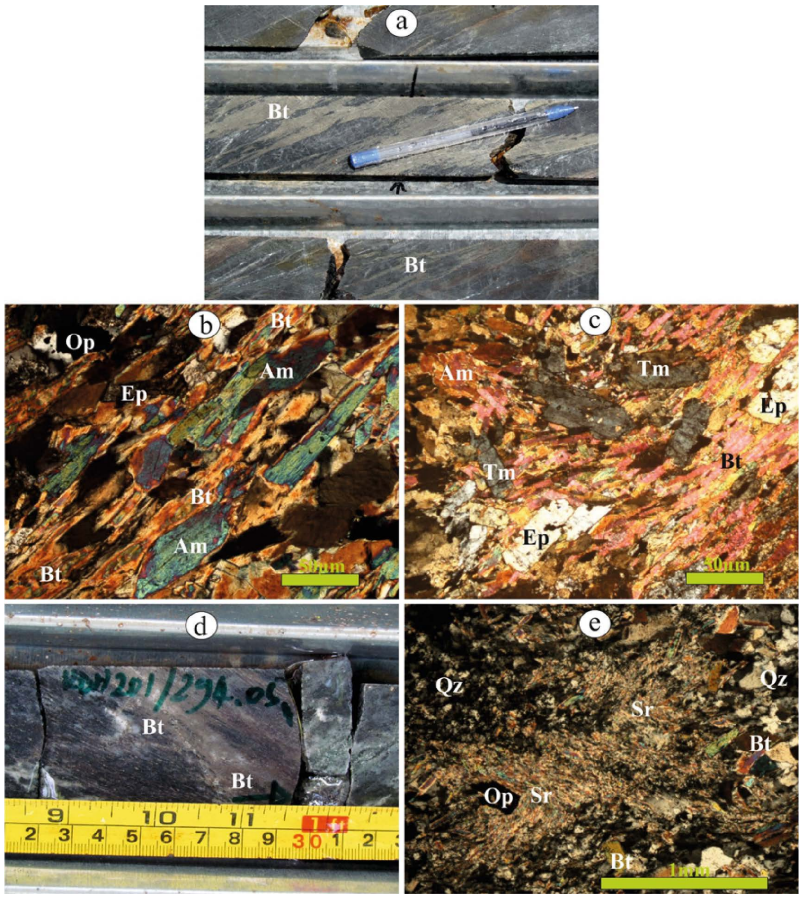

Figure 6. Photographs and photomicrographs of potassic alteration (cross-polarized light). (a) Amphibolite affected by potassic alteration (corresponded to sample KDH258-6, see location in Figure 3.) (b) Progressive replacement of amphibole (hornblende) by biotite. (c) Destabilization of amphibole to biotite and epidote, with crystallization of accessory tourmaline in sample KDH258-8. (d) Meta-microdiorite affected by biotitic potassic alteration. (e) Destabilization of feldspar phenocryst to sericite in metasediments. Am = amphibole, Bt = biotite, Ep = epidote, Op = opaque minerals, Pl = plagioclase, Qz = quartz, Sr = sericite, Tm = tourmaline.

In microdiorite, potassic alteration is also characterized by a biotitization highlighted by the crystallization of thin brownish biotite flakes, disseminated in quartz veinlets or abundant in mylonitized zones of the rock (Figure 6(d)).

Otherwise in metasediments, potassic alteration is characterized by an important development of very thin sheets of white mica (sericite) deriving from the destabilization of primary sheet minerals (biotite and muscovite) and feldspar that probably might be potassic (Figure 6(e)).

4.2.2. Chloritization

This alteration is spatially less extended than the potassic alteration. Chlorite is developed in fine-grained flakes clustered along the cleavage planes. These clusters form stretched and greenish lenticular patches that are clearly distinct from the relatively unaltered parts (Figure 7(a)). The chloritization is superimposed to the potassic-altered beds. In amphibolite, we observe a strong destabilization of biotite that is altered to chlorite, but relicts of biotite remain in chlorite clusters

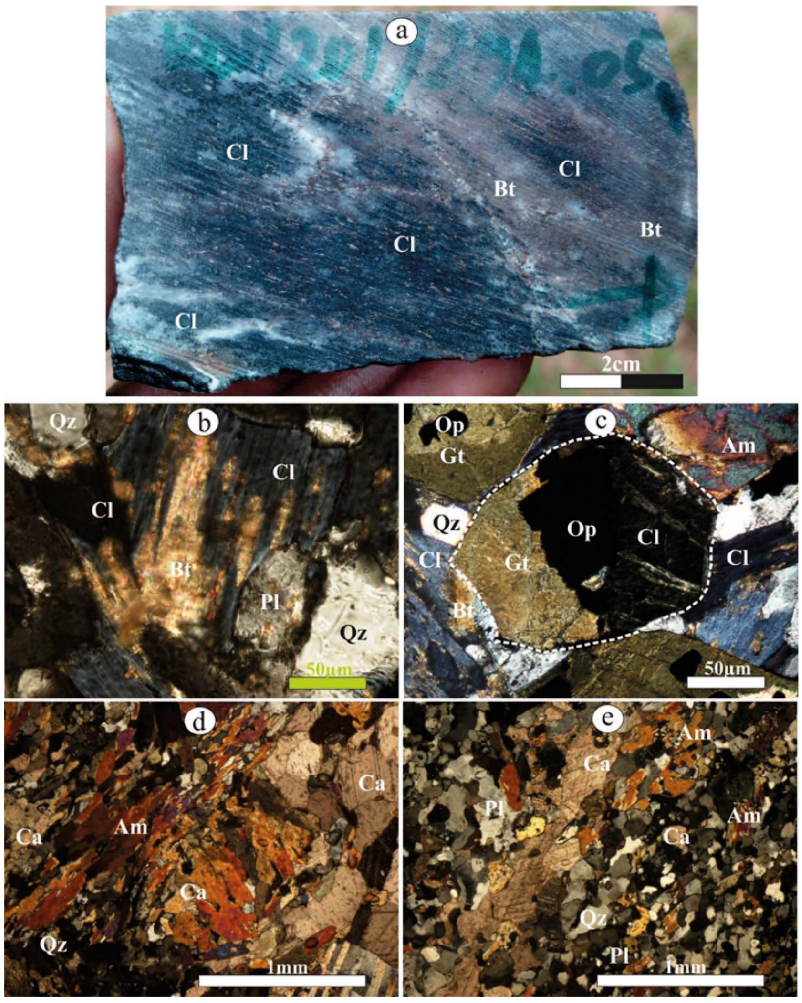

Figure 7. Chloritization and carbonation. (a) Macroscopic aspect of biotite chloritization in a metadiorite (cross-polarized light, corresponded to sample KDH258-7 see location in Figure 3). (b) Partial replacement of biotite by chlorite in amphibolite. (c) Chloritization garnet in amphibole. (d) Pseudomorphose of amphibole and plagioclase to massive calcite in amphibolite. (e) Carbonation of amphibole and plagioclase in meta-microdiorite. Am = amphibole, Bt = biotite, Cl = chlorite, Ca = carbonate, Gt = garnet, Op = opaque minerals, Pl = plagioclase, Qz = quartz.

(Figure 7(b)). The chloritization is accompanied by a soft silicification, characterized by recrystallized quartz that is interstitial between chlorite flakes. Garnet is partially affected by chloritization, leaving opaque relicts (Figure 7(c)). Pyrrhotite, chalcopyrite and pyrite are the sulfides associated with this alteration.

4.2.3. Carbonation

This alteration occurs lately relative to the other alterations. It is observed in all parts of the deposit, and independent of the nature of lithologies. It is generally observed as a diffuse replacement of amphibole and plagioclase by calcite (Figure 7(d) and Figure 7(e)), and also the emplacement of carbonate and quartz-carbonate veins. The quartz-carbonate veins are concordant or discordant to the regional fabric.

4.2.4. Mineralogical Evolution and Paragenesis

The mineral paragenesis of hydrothermal alterations that escort gold mineralization is expressed by the mineralogical evolution from the distal zone to the mineralization (Figure 8). This paragenesis was characterized by a detailed petrographic study of hole KDH258 (see Figure 3), which intersected only amphiboles.

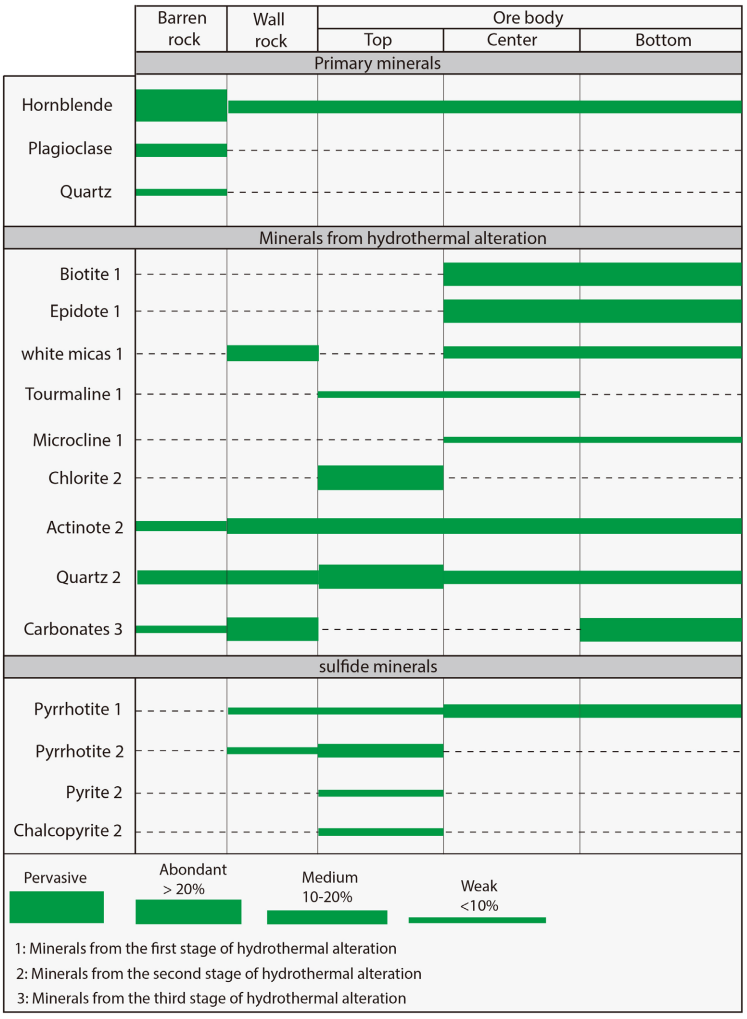

Figure 8. Mineral paragenesis associated with gold mineralization in amphibolitic rocks.

From the hanging wall to the bottom, major hornblende and plagioclase are progressively replaced by biotite and chlorite. The chemical balance of the minerals involved in this replacement matches the reactions of the Equations (1.1) and (1.2).

$$Ca\text{-}(Fe,Mg)\text{-}amphibole + fluid + K^{+} \rightarrow biotite + Ca - epidote(+Na + ?). \quad (1.1)$$

$$Ca\text{-}plagioclase + fluid + K^{+} \rightarrow illite(sericite) + Ca\text{-}epidote\left(+Na^{+} ?\right). \quad (1.2)$$

In the upper part of the mineralized body, we notice the presence of tourmaline, then with chloritization the occurrence of chalcopyrite and a second generation of pyrite. A transformation of biotite to chlorite implies a release of Si (atomic ratio Si/Al = 3 for biotite, and Si/Al = 2/3 for clinochlore-chamosite solid solution) that explains the abundance of quartz in the top wall of the mineralization. It also implies the mobility of K during this hydrothermal phase, as well as Fe and Mg that could be incorporated in oxides. On another note, the transformation of garnet to chlorite needs an input of Fe and Mg if we suppose that the Al content does not vary. Then, Fe and Mg are probably allocated to neoformed chlorite. Representative reactions of this alteration are proposed as follows:

$$biotite + fluid \rightarrow chlorite + Si^{4+}(quartz) + (Fe,Mg)^{2+} + K^{+}. \quad (2.1)$$

$$garnet + fluid + (Fe,Mg)^{2+} \rightarrow chlorite. \quad (2.2)$$

Since Fe and Mg content might not be added to the system but internally redistributed between mineral phases, the presence of fluid is insignificant for the achievement of this reaction.

The carbonates are located on the upper hanging wall, but also in the lower part of the mineralized zone. They replace amphibole and plagioclase, suggesting the incorporation of Ca, Mg and Fe in carbonate minerals, (Equation (3)), but particularly a release of Fe that can be integrated in oxides, or precipitating sulfides.

$$Ca\text{-}(Fe,Mg)\text{-}amphibole + Ca\text{-}Na\text{-}plagioclase + fluid + CO_2 \rightarrow (Ca,Fe,Mg)\text{-}carbonates + quartz + Al^{3+}\left(+Na^{+}\right). \quad (3)$$

Overall, major mineralogic changes are driven by input of K during potassic alteration, and the input of carbonate during carbonation. The behavior of Na is poorly constrained because of the absence of a Na-rich major minerals involved in hydrothermal alterations.

4.3. Hydrothermal Alteration and Mineralization Link

The observed sulfide mineralization is in accordance with the three hydrothermal stages of mineralization. The first mineralization stage is characterized by a potassic alteration, which one is preceded by a ductile deformation which affected amphibolite and metasediments. This deformation is highlighted by a slate cleavage S1, characterized by the orientation of amphibolite that is partially replaced by biotite, and crystallization of disseminated pyrrhotite. Pyrrhotite crystal is partially stretched and oriented along S1 cleavage (**Figure 9(c)**).

The second mineralization stage is synchronous with chloritization. It is

characterized by pyrrhotite, chalcopyrite and rare pyrite crystallization. Pyrrhotite is observed in two habits: (i) as fine crystals disseminated in chloritized layers associated with tourmaline, as inclusion in chloritized garnet porphyroclasts (**Figure 9(g)**), or also located in pressure shadows around garnet or tourmaline (**Figure 9(h)**); (ii) as 0.25 mm-wide trails, more than 2 mm-long following the slaty cleavage (**Figure 9(f)**). Chalcopyrite and pyrite replace partially pyrrhotite, (**Figure 9(a)** and **Figure 9(b)**) with pyrite manifesting in the form of microveins (**Figure 9(b)**). This mineralization phase is associated with ductile-fragile context characterized by the formation of asymmetric pressure shadows (**Figure 9(h)**).

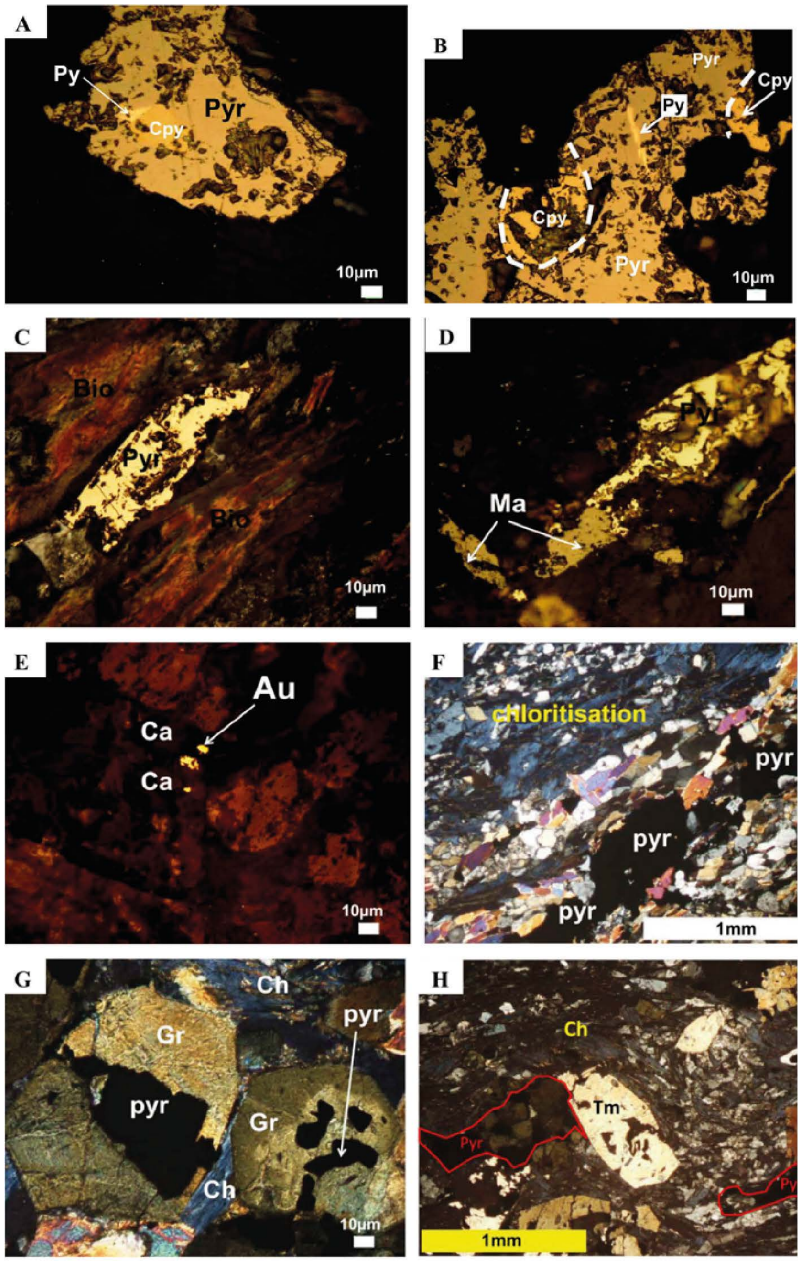

Figure 9. Sulfides and metals associated with different types of hydrothermal alteration.

The third phase is related to the carbonation and the silicification as veins quartz in the walls of the mineralization, that are sheltered by pyrrhotite. This mineralization is emphasized by abundant crystallization of pyrrhotite, and very fine micrometric gold particles (Figure 9(c)).

4.4. Geochemical Characterization of the Mineralization

We compared majors and trace elements composition between the barren samples and the mineralized samples of the KDH258 drilling (Table 1). The Al_2O_3 and Fe_2O_3 content does not vary too much between the barren and the mineralized zones (Figure 10(a)). The highest loss on ignition (LOI) values are found around the mineralized body (from KDH258-3 to KDH258-9). The mineralized body is also characterized by higher content in K_2O, Rb and Cs (Figure 10(a) and Figure 10(b)). This is consistent with potassic alteration in the mineralized zone and the geochemical behavior of Rb and Cs that is similar to that of K. Besides, we can observe a depletion of P_2O_5 and LREE toward the mineralized body. HREE is not too different in composition between the mineralized body and the surrounding amphibolite. Still, the top of the mineralized body possesses a higher HREE content than the bottom. The highest content of As (281 ppm) and Cu (170 ppm) are found in the mineralized body, but essential Cu content is also found in the surrounding rocks (130 ppm in the upper side, 90 ppm in the lower side).

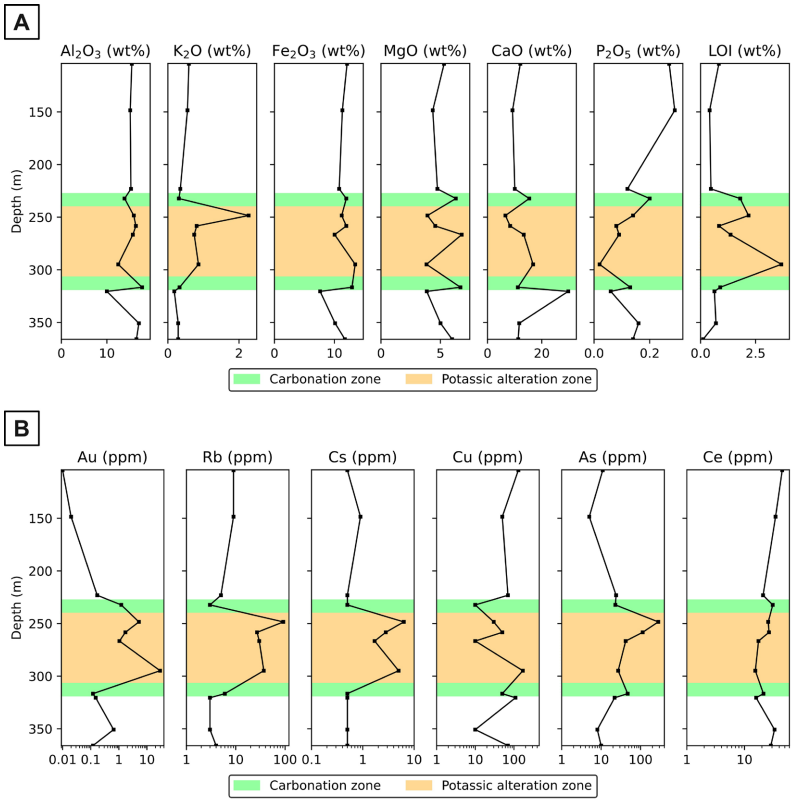

Figure 10. Major and trace compositions according to the depth. Potassic and carbonatic alteration zones are inferred from geochemical composition. (A) Major oxides compositions. (B) Trace elements composition.

Table 1. Chemical compositions of the samples (major and trace elements).

Samples		KDH 258-1	KDH 258-2	KDH 258-3	KDH 258-4	KDH 258-6	KDH 258-7	KDH 258-8	KDH 258-9	KDH 258-10	KDH 258-11	KDH 258-12	KDH 258-13
Position		Top	Top	Top	Top	Ore	Ore	Ore	Ore	Bottom	Bottom	Bottom	Bottom
Depth (m)		104.3	148.5	223.15	232.3	248.45	258.35	266.6	294.8	316.6	320.48	350.78	365.92
SiO_2		48.64	53.89	52.52	47.59	54.5	52.65	50.15	46.18	46.86	29.85	49.92	50
Al_2O_3		15.48	15.12	15.28	13.88	15.9	16.36	15.7	12.49	17.72	9.99	17.02	16.49
Fe_2O_3		12.1	11.32	10.79	11.98	11.21	11.98	10.04	13.45	12.92	7.61	10.11	11.74
MnO		0.178	0.213	0.183	0.229	0.115	0.13	0.196	0.166	0.188	0.312	0.214	0.17
MgO		5.31	4.36	4.75	6.3	3.91	4.57	6.79	3.83	6.69	3.85	5.01	5.98
CaO	wt%	12.08	9.21	10.06	15.37	6.6	8.33	13.37	16.79	11.2	29.74	11.7	11.3
Na_2O		2.64	4.26	3.94	2.06	2.49	3.39	1.7	1.44	3.1	1.6	3.36	3.25
K_2O		0.59	0.55	0.35	0.31	2.27	0.81	0.74	0.86	0.33	0.18	0.29	0.29
TiO_2		1.055	1.09	0.734	0.876	0.809	0.777	0.743	0.566	0.826	0.452	0.812	0.749
P_2O_5		0.27	0.29	0.12	0.2	0.14	0.08	0.09	0.02	0.13	0.06	0.16	0.14
LOI		0.83	0.41	0.47	1.8	2.18	0.84	1.36	3.67	0.89	0.63	0.7	0.12
Au[a]		0.01	0.02	0.17	1.22	5.15	1.71	1.05	29.3	0.12	0.15	0.65	0.12
Ga		19	16	17	16	17	17	16	14	18	10	16	17
Sc		30	28	47	50	45	46	40	38	53	31	42	46
V		218	173	261	288	230	205	220	223	271	161	223	240
Ba		107	192	234	66	584	208	144	117	163	70	137	154
Sr		521	552	365	384	366	452	448	272	321	311	462	381
Y		19	21	21	29	24	23	18	16	24	21	21	21
Zr		80	72	46	49	51	46	41	42	47	29	55	53
Cr		480	370	270	230	270	260	250	190	270	150	220	230
Co		62	36	74	31	70	52	28	52	55	34	32	45
Ni		310	190	150	120	130	100	100	150	90	70	60	90
Cu	ppm	130	50	70	10	30	50	10	170	50	110	10	70
Zn		120	270	130	110	100	170	100	90	90	80	90	90
As		11	5	24	23	281	113	42	27	47	22	8	10
Rb		9	9	5	3	92	27	30	37	6	3	3	4
Sb		1.9	1	1.2	1.9	2.5	2	2	1.8	2.1	1.3	1.8	1.8
Cs		0.5	0.9	0.5	0.5	6.3	2.8	1.7	5	0.5	0.5	0.5	0.5
Hf		2.1	2.1	1.3	1.6	1.6	1.3	1.2	1.3	1.4	0.7	1.6	1.4
Ta		0.3	0.2	0.1	0.2	0.2	0.1	0.2	0.1	0.2	0.1	0.2	0.4
W		7	6	11	57	8	14	16	13	5	8	14	31
Th		1.5	1.1	0.8	0.9	0.8	0.7	0.6	0.6	0.6	0.3	1	0.9
U		0.5	0.3	0.4	0.7	0.2	0.2	0.2	0.1	0.4	0.2	0.5	0.3

Continued

La	ppm	18	13.2	7.8	12	9.5	10.4	6.7	7	8.2	6.5	13.1	10.9
Ce		45.1	34.6	21	30.9	25.8	26.6	17.5	15.4	21.3	15.9	33.2	28.6
Pr		6.05	4.74	3.03	4.19	3.63	3.53	2.49	1.91	2.95	2.13	4.57	3.9
Nd		26.4	20.9	13.9	19.2	17.3	16.2	11.5	8.1	13.9	9.5	19.7	17.2
Sm		5.4	4.5	3.3	4.4	3.7	3.4	2.7	1.7	3.2	2.3	3.9	3.4
Eu		1.53	1.34	0.98	1.53	0.95	0.94	1.01	0.78	0.89	1.05	1.23	1.2
Gd		4.7	4.6	3.9	4.9	4.6	4.1	3.1	2.1	3.8	2.8	3.8	3.6
Tb		0.7	0.7	0.7	0.8	0.7	0.7	0.5	0.4	0.6	0.5	0.6	0.6
Dy		3.9	4.1	4.1	5.5	4.6	4.5	3.3	2.5	4.1	3.2	3.9	3.8
Ho		0.8	0.8	0.9	1.2	1	0.9	0.7	0.6	0.9	0.7	0.8	0.8
Er		2.2	2.4	2.7	3.6	2.9	2.8	2.1	2	2.8	2.3	2.5	2.4
Tm		0.34	0.35	0.41	0.55	0.43	0.42	0.33	0.34	0.44	0.38	0.4	0.38
Yb		2.2	2.3	2.9	3.9	2.7	2.7	2.3	2.4	3.1	2.5	2.8	2.5
Lu		0.33	0.33	0.45	0.61	0.41	0.42	0.34	0.38	0.51	0.38	0.42	0.39

a. Au content provided by the company.

The geochemical characterization of the described alterations was accomplished by applying Principal Components Analysis (PCA). PCA extracts the underlying factors that control correlations and variance among chemical elements, facilitating the clustering of these elements into distinct groups. The analysis was conducted considering major oxides, loss on ignition, Au, rare earth elements reduced to Ce (for LREE), Eu, Gd (for MREE) and Yb (HREE), and other trace elements. Each variable was scaled before component calculation using a Z-score normalization for the calculation. For better coherence of the results, we remove two samples from the calculation, the sample KDH258-4 and KDH258-11. The sample KDH258-4 differs from the other samples by its high content in trace elements such as Y, W, U, HREE, which can be accounted for the presence of accessory phases enriched in these elements. The sample KDH258-11 is quite different from the other samples by its major element's composition by its lower content in SiO_2, Al_2O_3, Fe_2O_3, MgO, K_2O, and higher content in CaO, Na_2O, MnO, meaning this sample is different from the other amphibolite samples of the drill hole.

The principal component analysis provides three principal components representing, 35.21%, 19.62%, and 17.92% of the variance of chemical elements, respectively.

The representation of component 1 vs component 2 (Figure 11) exposes three groups of chemical elements. The group composed of K2O, Ba, Rb, Cs, and As lies in the upper left part of the representation, and K2O, Ba, Rb, Cs, and As lies in the upper left part of the representation and relates to the potassic alteration. A second group in the center right part of the representation is composed of a dense cluster of P_2O_5, TiO_2, Na_2O, Cs, and high field strength elements (HFSE) such as Eu, Zr,

Ce, Th, Sr, Hf. This second group is opposed to LOI and Au in component 1. Then which might be related to a highly mineralizing hydrothermal alteration stage that should correspond with the carbonation. The third group is sparsely extended in the lower part of the representation and is composed of CaO, MnO, Cu, and to a lesser extent MgO, W, and Fe_2O_3.

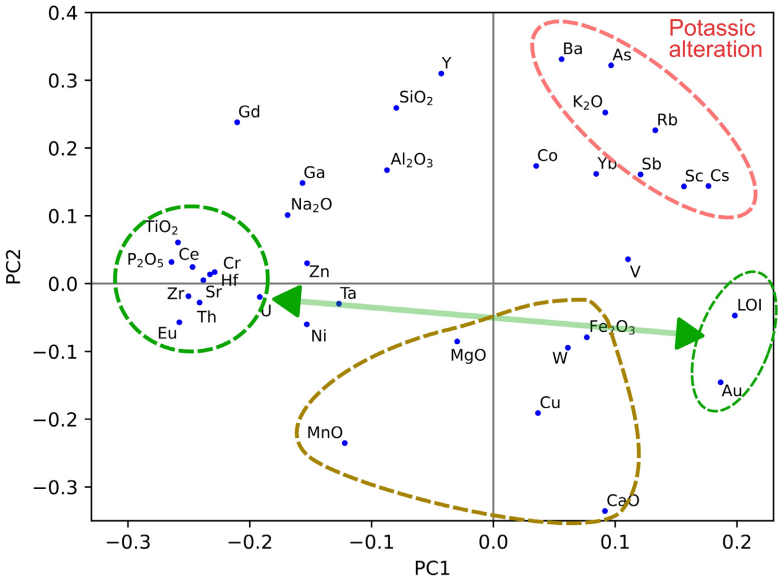

Figure 11. Principal Component Analysis (PCA) plot of geochemical elements relative to components 1 and 2.

5. Discussion

5.1. Metamorphism-Related Processes

The Kiaka gold deposit is hosted in a variety of surrounding rocks. The main facies are amphibolite, metamicrodiorite and metasediments. These formations are affected by a prograde metamorphism that reached the amphibolite facies, and a retrometamorphism in greenschists facies. (i) The amphibolite facies are recorded in amphibolite by the paragenesis amphibole-plagioclase-garnet [33] [66] [67]. It is characterized by a contact metamorphism between granitoids and metamorphic units of the greenstones belt [33] [38] [52] [66], consistent with an isobaric heating at 7.5 kbar up to 550˚C [12] [57]. (ii) The retro metamorphism in greenschist facies conditions is featured in amphibolite by the destabilization of hornblende into actinote and by pseudomorphs of hornblende to carbonate. These figures of pseudomorphosis were previously reported in Kiaka. In such a setting, hydrothermal and mineralization processes might occur during the metamorphism retrograde path [5] [48].

5.2. Geochemical Processes and Structural Regime

The geochemistry of the altered surrounding rocks provides information about the nature of the hydrothermal fluids responsible for the mineralization, and can

be linked to the structural context of the mineralization.

(i) The first hydrothermal phase is potassic. It is associated with ductile deformation highlighted by an S1 slate cleavage. The geochemical overprint of this alteration is highlighted by an increase of K_2O, accompanied by enrichment in Cs, Rb, As and Ba. A depletion of Na_2O during this alteration phase would be consistent with the chemical balance of the Equations (1.1) and (1.2), but geochemical data suggest that its depletion is mainly related to the carbonation (discussed below).

(ii) The microstructural studies put in evidence shearing structures (porphyroclasts and pressure shadows, **Figure 9**), and pyrrhotite veinlets associated with this second phase of fluid circulation. These shear structures highlight a ductile-brittle rheology during this hydrothermal alteration phase. This second alteration phase is concurrent with a second phase of mineralization dominated by precipitation of the second generation of pyrrhotite, as dissemination or in trails between slate cleavage. Since no significant change in SiO_2, the Si that might be released by chloritization of biotite (Equation (2)) is not extracted from the system and probably recrystallized in quartz. Also, the MgO and Fe_2O_3 content of the mineralized body remains in the average range of composition, implying that Fe and Mg behaved as immobile elements during the alterations. We then deduce that no Mg or Fe content was added or lost during the chloritization, and later carbonation phase.

(iii) The third phase of fluid circulation happens lately in the brittle deformation context, as suggested by the opening of carbonate- and quartz-bearing veins, also accompanied by a diffused carbonation in the surrounding rock. We assume that this alteration is depicted by the LOI composition, which certainly encompasses CO_2 content, since C was not analyzed samples. The high Au strongly correlates with the LOI, suggesting that the most important mineralizing phase is related to carbonation. At the same time, we observe a depletion in P_2O_5, TiO_2, and Na_2O, and HFSE with increasing LOI. Their opposition to PCA suggests that these elements are mostly depleted during the carbonation phase. The late character of this alteration, combined with brittle deformation, probably played an important role in the remobilization and reconcentration of gold in favorable traps. A structural control could explain why the mineralization is located in the potassic-altered zone whereas carbonation covers a large zone around the mineralized body.

5.3. Significance of the Kiaka Gold Deposit Alterations

The potassic alteration identified in the Kiaka gold deposit is a common signature observed in gold deposit, typified by an alkali metasomatism and large ionic lithophile elements (LILE) enrichment [70]-[72]. In our case study, only K is involved in this early alteration, like in the Sergozero gold prospect in Fennoscandian Shield, Finland [73]. This type of alteration is consistent with the circulation of high-temperature fluids (superior to 400˚C) [8], in amphibolite to greenschist

facies environment, which favors the stabilization of biotite over white mica [72]. Potassium-rich fluids are often suggested as deriving from felsic melt in the lower crust, with metal input from the leached formations traversed by the fluids [74] [75]. The apparent deficiency of Na relative to K as alkali-dominant component allows us to rule out sodic alkaline intrusions as possible source of hydrothermal fluids, as proposed for albitized gold deposits (e.g. [75]). Although many West African gold deposits are associated with dioritic bodies [48] [52] [76]-[78], and linkage of potassic fluid with dioritic bodies in Kiaka is hardly reliable, knowing that the dioritic body in Kiaka (2140 ± 8 Ma by U-Pb on zircon) postdates the early mineralization stage (2157 ± 24 Ma). This conclusion is also supported by [79] basing also their conclusion on boron isotopes in tourmaline. Nevertheless, they do not evoke a possible deep magmatic-anatectic source, but rather a devolatilization of muscovite-hosting metasediments. Considering the that the genesis of anatectic and magmatic bodies in the lower part of the crust occurs regionally and over a large time period [40], it can be conceived that some K-rich fluids could derive entirely or partially from the deeper zone of magmatic intrusions or anatectic zones, with a transport favored by shear zones. Besides this, mineralization is accompanied by the potassic alteration, with precipitation of the first generation of pyrrhotite, and low-grade gold.

The intense chloritization which characterizes the second hydrothermal phase can be attributed to a retrograde transformation of biotite in chlorite. We deduced from the geochemical analysis that there is no significant change in Mg and Fe content in the rock during the chloritization, which is consistent with a metamorphism-induced alteration. However, the occurrence of chloritization as lenticular patches imply a significant influence from circulating hydrothermal fluids. Probably, hydrothermal fluids interplay with the prevailing the pressure-temperature conditions to enhance the retrogressive transformation of biotite to chlorite. Similar retrograde alteration is identified in gold-bearing amphibolitic formations in the Kibi-Winneba belt, south-west of Ghana, that was explained by a retrograde post-peak metamorphism alteration [5]. In the Tonbado gold prospect (center of Ivory Coast), chloritization was also linked to greenschist metamorphic facies [80]. In the Yalea deposit (Loulo gold district, Mali), chloritization is accompanied by sericitization [81], in contrast to our case study where sericitization occurred in the first hydrothermal stage. This indicates a decrease in the chemical activity of alkalis (principally K) transitioning from potassic alteration to chloritization.

The carbonation phase implies the circulation of a fluid with a high CO_2 activity, generally a aqueous-carbon low salinity fluid [82] that would provoke the transformation of ferromagnesian minerals to calcite, dolomite and ankerite, and also heighten the precipitation of sulfurs. The carbonation was related to a brittle tectonic setting, likewise with the gold deposits of Bombore (in the north of Kiaka district) and Nabenia (near Tiebele, in the south of south of Kiaka district) of and Bombore, along NE-SW shear zones. [83] highlighted that in archean Yilgarn

Craton, carbonation is more extended than potassic alteration in greenschist facies related deposit, contrary to amphibolite facies related deposit where potassic alteration is more dispersed. Following a similar setting, carbonation occurred in Kiaka during a retrograde greenschist metamorphism, with transition to a brittle deformation regime.

Sulfidation occurs in all the identified hydrothermal alterations, with pyrrhotite as the main iron-sulfide oxide. We only observed a sulfide diversification during chloritization, resulting from replacement of pyrrhotite by chalcopyrite and pyrite. This change is consistent with a shift of the hydrothermal fluid composition during chloritization. In the same stability domain with chalcopyrite, a change to a more oxidized fluid favors the replacement of pyrrhotite to pyrite [84]. Copper analyses do not reveal a change in its concentration between the borders and the mineralized body. If we exclude the hypothesis that an extensive metasomatism brought Cu into the amphibolite, we can narrow it down to the hypothesis that copper is mobilized directly from the host rocks, during retrograde metamorphism, to be incorporated into chalcopyrite. According to [12], a disseminated gold mineralization occurs during this chloritization.

The carbonation can be related to the late gold-rich alteration stage of [12], that is associated in greywacke with arsenopyrite replacing pyrrhotite, and löllingite in greywacke. In our case study, As is among the elements enriched with potassic alteration. This suggests that either as is early mobilized with potassic alteration and associated with pyrrhotite-1, or that potassic-altered bodies possess geochemical features that enhance the precipitation of As from CO_2-rich fluids. In both cases, As was incorporated in pyrrhotite.

Sericitization seems to be an alteration process primarily distinctively associated with metasedimentary host rocks, as it is described by [12], but not in our observed amphibolite. This feature is common in many gold-rich terranes, such as in the Egyptian eastern desert [85].

6. Conclusion

We described three alteration stages in the Kiaka gold deposit (potassic alteration, chloritization, and carbonation) that highlighted a transition from a ductile to fragile regime, but only two hydrothermal stages seem to account for the major geochemical changes in the mineralized bodies and surrounding rocks. We link the first hydrothermal alteration with K-rich hydrothermal fluids that induced a biotitization of mafic rocks, with enrichment in LILE elements, Au and As. The alteration occurs during a ductile deformation regime. The chloritization depicts the onset of retrograde metamorphism, and a decrease of alkali content in hydrothermal fluids, without a significant change in Fe and Mg content. This stage culminates with a high activity of CO_2, responsible for carbonation of the surrounding rocks. Remobilization of Au and other trace elements (Na, P, HFSE) are related to this late carbonation stage. It occurs during a transition from ductile to a fragile regime.

Conflicts of Interest

The authors declare no conflicts of interest regarding the publication of this paper.

References

[1] Robertson, M. and Peters, L. (2016) West African Goldfields. *Episodes*, **39**, 155-176. https://doi.org/10.18814/epiiugs/2016/v39i2/95773

[2] Béziat, D., Dubois, M., Debat, P., Nikiéma, S., Salvi, S. and Tollon, F. (2008) Gold Metallogeny in the Birimian Craton of Burkina Faso (West Africa). *Journal of African Earth Sciences*, **50**, 215-233. https://doi.org/10.1016/j.jafrearsci.2007.09.017

[3] Goldfarb, R.J., André-Mayer, A., Jowitt, S.M. and Mudd, G.M. (2017) West Africa: The World's Premier Paleoproterozoic Gold Province. *Economic Geology*, **112**, 123-143. https://doi.org/10.2113/econgeo.112.1.123

[4] Bamba, O., Beziat, D., Bourges, F., Debat, P., Lompo, M., Parizot, J., *et al.* (1997) Nouveau type de gisement aurifère dans les ceintures de roches vertes birimiennes du Burkina Faso: Les albitites de Larafella. *Journal of African Earth Sciences*, **25**, 369-381. https://doi.org/10.1016/s0899-5362(97)00110-3

[5] Klemd, R., Hünken, U. and Olesch, M. (2002) Metamorphism of the Country Rocks Hosting Gold-Sulfide-Bearing Quartz Veins in the Paleoproterozoic Southern Kibi-Winneba Belt (SE-Ghana). *Journal of African Earth Sciences*, **35**, 199-211. https://doi.org/10.1016/s0899-5362(02)00122-7

[6] Baratoux, L., Metelka, V., Naba, S., Ouiya, P., Siebenaller, L., Jessell, M.W., *et al.* (2015) Tectonic Evolution of the Gaoua Region, Burkina Faso: Implications for Mineralization. *Journal of African Earth Sciences*, **112**, 419-439. https://doi.org/10.1016/j.jafrearsci.2015.10.004

[7] Cathelineau, M., Boiron, M.-C. and Tuduri, J. (2011) Fluides et genèse des concentrations minérales. *Géosciences*, **13**, 56-63.

[8] Pirajno, F. (2009) Hydrothermal Processes and Wall Rock Alteration. In: Pirajno, F., Ed., *Hydrothermal Processes and Mineral Systems*, Springer, 73-164. https://doi.org/10.1007/978-1-4020-8613-7_2

[9] Beaudoin, G., Therrien, R. and Savard, C. (2006) 3D Numerical Modelling of Fluid Flow in the Val-D'or Orogenic Gold District: Major Crustal Shear Zones Drain Fluids from Overpressured Vein Fields. *Mineralium Deposita*, **41**, 82-98. https://doi.org/10.1007/s00126-005-0043-5

[10] Goldfarb, R.J., Baker, T., Dubé, B., Groves, D.I., Hart, C.J.R. and Gosselin, P. (2005) Distribution, Character, and Genesis of Gold Deposits in Metamorphic Terran. In: Hedenquist, J.W., Thompson, J.F.H., Goldfarb, R.J. and Richards, J.P., Eds., *One Hundredth Anniversary Volume*, Society of Economic Geologists, 405-450. https://doi.org/10.5382/av100.14

[11] Groves, D.I., Goldfarb, R.J., Gebre-Mariam, M., Hagemann, S.G. and Robert, F. (1998) Orogenic Gold Deposits: A Proposed Classification in the Context of Their Crustal Distribution and Relationship to Other Gold Deposit Types. *Ore Geology Reviews*, **13**, 7-27. https://doi.org/10.1016/s0169-1368(97)00012-7

[12] Fontaine, A., Eglinger, A., Ada, K., André-Mayer, A., Reisberg, L., Siebenaller, L., *et al.* (2017) Geology of the World-Class Kiaka Polyphase Gold Deposit, West African Craton, Burkina Faso. *Journal of African Earth Sciences*, **126**, 96-122. https://doi.org/10.1016/j.jafrearsci.2016.11.017

[13] Hammond, N.Q., Robb, L., Foya, S. and Ishiyama, D. (2011) Mineralogical, Fluid Inclusion and Stable Isotope Characteristics of Birimian Orogenic Gold Mineralization

at the Morila Mine, Mali, West Africa. *Ore Geology Reviews*, **39**, 218-229. https://doi.org/10.1016/j.oregeorev.2011.03.002

[14] Grenholm, M., Jessell, M. and Thébaud, N. (2019) A Geodynamic Model for the Paleoproterozoic (ca. 2.27-1.96 Ga) Birimian Orogen of the Southern West African Craton—Insights into an Evolving Accretionary-Collisional Orogenic System. *Earth-Science Reviews*, **192**, 138-193. https://doi.org/10.1016/j.earscirev.2019.02.006

[15] Tapsoba, B., Lo, C., Jahn, B., Chung, S., Wenmenga, U. and Iizuka, Y. (2013) Chemical and Sr-Nd Isotopic Compositions and Zircon U-Pb Ages of the Birimian Granitoids from NE Burkina Faso, West African Craton: Implications on the Geodynamic Setting and Crustal Evolution. *Precambrian Research*, **224**, 364-396. https://doi.org/10.1016/j.precamres.2012.09.013

[16] Abouchami, W., Boher, M., Michard, A. and Albarede, F. (1990) A Major 2.1 Ga Event of Mafic Magmatism in West Africa: An Early Stage of Crustal Accretion. *Journal of Geophysical Research: Solid Earth*, **95**, 17605-17629. https://doi.org/10.1029/jb095ib11p17605

[17] Boher, M., Abouchami, W., Michard, A., Albarede, F. and Arndt, N.T. (1992) Crustal Growth in West Africa at 2.1 Ga. *Journal of Geophysical Research: Solid Earth*, **97**, 345-369. https://doi.org/10.1029/91jb01640

[18] Doumbia, S., Pouclet, A., Kouamelan, A., Peucat, J.J., Vidal, M. and Delor, C. (1998) Petrogenesis of Juvenile-Type Birimian (Paleoproterozoic) Granitoids in Central Côte-d'Ivoire, West Africa: Geochemistry and Geochronology. *Precambrian Research*, **87**, 33-63. https://doi.org/10.1016/s0301-9268(97)00201-5

[19] Gasquet, D., Barbey, P., Adou, M. and Paquette, J.L. (2003) Structure, Sr-Nd Isotope Geochemistry and Zircon U-Pb Geochronology of the Granitoids of the Dabakala Area (Côte d'Ivoire): Evidence for a 2.3 Ga Crustal Growth Event in the Palaeoproterozoic of West Africa? *Precambrian Research*, **127**, 329-354. https://doi.org/10.1016/s0301-9268(03)00209-2

[20] Pawlig, S., Gueye, M., Klischies, R., Schwarz, S., Wemmer, K. and Siegesmund, S. (2006) Geochemical and Sr-Nd Isotopic Data on the Birimian of the Kedougou-Kenieba Inlier (Eastern Senegal): Implications on the Palaeoproterozoic Evolution of the West African Craton. *South African Journal of Geology*, **109**, 411-427. https://doi.org/10.2113/gssajg.109.3.411

[21] Sakyi, P.A., Addae, R.A., Su, B., Dampare, S.B., Abitty, E., Su, B., *et al.* (2020) Petrology and Geochemistry of TTG and K-Rich Paleoproterozoic Birimian Granitoids of the West African Craton (Ghana): Petrogenesis and Tectonic Implications. *Precambrian Research*, **336**, Article 105492. https://doi.org/10.1016/j.precamres.2019.105492

[22] Taylor, P.N., Moorbath, S., Leube, A. and Hirdes, W. (1992) Early Proterozoic Crustal Evolution in the Birimian of Ghana: Constraints from Geochronology and Isotope Geochemistry. *Precambrian Research*, **56**, 97-111. https://doi.org/10.1016/0301-9268(92)90086-4

[23] Baratoux, L., Metelka, V., Naba, S., Jessell, M.W., Grégoire, M. and Ganne, J. (2011) Juvenile Paleoproterozoic Crust Evolution during the Eburnean Orogeny (~2.2-2.0 ga), Western Burkina Faso. *Precambrian Research*, **191**, 18-45. https://doi.org/10.1016/j.precamres.2011.08.010

[24] Grenholm, M., Jessell, M. and Thébaud, N. (2019) Paleoproterozoic Volcano-Sedimentary Series in the Ca. 2.27 - 1.96 Ga Birimian Orogen of the Southeastern West African Craton. *Precambrian Research*, **328**, 161-192. https://doi.org/10.1016/j.precamres.2019.04.005

[25] Hirdes, W., Davis, D.W., Lüdtke, G. and Konan, G. (1996) Two Generations of Birimian (Paleoproterozoic) Volcanic Belts in Northeastern Côte d'Ivoire (West Africa): Consequences for the 'Birimian Controversy'. *Precambrian Research*, **80**, 173-191. https://doi.org/10.1016/s0301-9268(96)00011-3

[26] Leube, A., Hirdes, W., Mauer, R. and Kesse, G.O. (1990) The Early Proterozoic Birimian Supergroup of Ghana and Some Aspects of Its Associated Gold Mineralization. *Precambrian Research*, **46**, 139-165. https://doi.org/10.1016/0301-9268(90)90070-7

[27] Milési, J.-P., Heinry, C. and Sylvain, J.-P. (1989) Minéralisations aurifères de l'Afrique de l'ouest leurs relations avec l'évolution lithostructurale au Proterozoique inférieur. Bureau de recherches géologiques et minières.

[28] Lompo, M. (2010) Paleoproterozoic Structural Evolution of the Man-Leo Shield (West Africa). Key Structures for Vertical to Transcurrent Tectonics. *Journal of African Earth Sciences*, **58**, 19-36. https://doi.org/10.1016/j.jafrearsci.2010.01.005

[29] Naba, S., Lompo, M., Debat, P., Bouchez, J.L. and Béziat, D. (2004) Structure and Emplacement Model for Late-Orogenic Paleoproterozoic Granitoids: The Tenkodogo-Yamba Elongate Pluton (Eastern Burkina Faso). *Journal of African Earth Sciences*, **38**, 41-57. https://doi.org/10.1016/j.jafrearsci.2003.09.004

[30] Parra-Avila, L.A., Kemp, A.I.S., Fiorentini, M.L., Belousova, E., Baratoux, L., Block, S., *et al.* (2017) The Geochronological Evolution of the Paleoproterozoic Baoulé-Mossi Domain of the Southern West African Craton. *Precambrian Research*, **300**, 1-27. https://doi.org/10.1016/j.precamres.2017.07.036

[31] Parra-Avila, L.A., Belousova, E., Fiorentini, M.L., Eglinger, A., Block, S. and Miller, J. (2018) Zircon Hf and O-Isotope Constraints on the Evolution of the Paleoproterozoic Baoulé-Mossi Domain of the Southern West African Craton. *Precambrian Research*, **306**, 174-188. https://doi.org/10.1016/j.precamres.2017.12.044

[32] Pons, J., Barbey, P., Dupuis, D. and Léger, J.M. (1995) Mechanisms of Pluton Emplacement and Structural Evolution of a 2.1 Ga Juvenile Continental Crust: The Birimian of Southwestern Niger. *Precambrian Research*, **70**, 281-301. https://doi.org/10.1016/0301-9268(94)00048-v

[33] Castaing, C., Billa, M., Milési, J., Thiéblemont, D., Le Metour, J., Egal, E., *et al.* (2003) Notice explicative de la Carte géologique et minière du Burkina Faso à 1/1,000,000. BRGM BUMIGEB.

[34] Lompo, M. (2009) Geodynamic Evolution of the 2.25-2.0 Ga Palaeoproterozoic Magmatic Rocks in the Man-Leo Shield of the West African Craton. a Model of Subsidence of an Oceanic Plateau. *Geological Society, London, Special Publications*, **323**, 231-254. https://doi.org/10.1144/sp323.11

[35] Parra-Avila, L.A., Baratoux, L., Eglinger, A., Fiorentini, M.L. and Block, S. (2019) The Eburnean Magmatic Evolution across the Baoulé-Mossi Domain: Geodynamic Implications for the West African Craton. *Precambrian Research*, **332**, Article 105392. https://doi.org/10.1016/j.precamres.2019.105392

[36] Hein, K.A.A. (2010) Succession of Structural Events in the Goren Greenstone Belt (Burkina Faso): Implications for West African Tectonics. *Journal of African Earth Sciences*, **56**, 83-94. https://doi.org/10.1016/j.jafrearsci.2009.06.002

[37] Lompo, M., Bourges, F., Debat, P., Lespinasse, P. and Bouchez, J.-L. (1995) Mise en place d'un pluton granitique dans la croûte birimienne fragile: Fabrique magnétique du massif de Tenkodogo (Burkina Faso). *Comptes rendus de l'Académie des sciences Série 2 Sciences de la terre et des planètes*, **320**, 1211-1218.

[38] Pons, J., Oudin, C. and Valero, J. (1992) Kinematics of Large Syn-Orogenic

Intrusions: Example of the Lower Proterozoic Saraya Batholith (Eastern Senegal). *Geologische Rundschau*, **81**, 473-486. https://doi.org/10.1007/bf01828610

[39] Traoré, A. (2011) Mise en place des plutons de granites alcalins paléoprotérozoïques du Burkina Faso (Afrique de l'Ouest). Ph.D. Thesis, Université de Ouagadougou.

[40] Bonzi, W.M., Vanderhaeghe, O., Van Lichtervelde, M., Wenmenga, U., André-Mayer, A., Salvi, S., *et al.* (2021) Petrogenetic Links between Rare Metal-Bearing Pegmatites and TTG Gneisses in the West African Craton: The Mangodara District of SW Burkina Faso. *Precambrian Research*, **364**, Article 106359. https://doi.org/10.1016/j.precamres.2021.106359

[41] Bossière, G., Bonkoungou, I., Peucat, J. and Pupin, J. (1996) Origin and Age of Paleoproterozoic Conglomerates and Sandstones of the Tarkwaian Group in Burkina Faso, West Africa. *Precambrian Research*, **80**, 153-172. https://doi.org/10.1016/s0301-9268(96)00014-9

[42] Davis, D.W., Hirdes, W., Schaltegger, U. and Nunoo, E.A. (1994) U-Pb Age Constraints on Deposition and Provenance of Birimian and Gold-Bearing Tarkwaian Sediments in Ghana, West Africa. *Precambrian Research*, **67**, 89-107. https://doi.org/10.1016/0301-9268(94)90006-x

[43] Koffi, Y.H., Wenmenga, U. and Djro, S.C. (2016) Tarkwaian Deposits of the Birimian Belt of Houndé: Petrological, Structural and Geochemical Study (Burkina-Faso, West Africa). *International Journal of Geosciences*, **7**, 685-700. https://doi.org/10.4236/ijg.2016.75053

[44] Traoré, K., Chardon, D., Naba, S., Wane, O. and Bouaré, M.L. (2022) Paleoproterozoic Collision Tectonics in West Africa: Insights into the Geodynamics of Continental Growth. *Precambrian Research*, **376**, Article 106692. https://doi.org/10.1016/j.precamres.2022.106692

[45] Chardon, D., Bamba, O. and Traoré, K. (2020) Eburnean Deformation Pattern of Burkina Faso and the Tectonic Significance of Shear Zones in the West African Craton. *BSGF—Earth Sciences Bulletin*, **191**, Article No. 2. https://doi.org/10.1051/bsgf/2020001

[46] Ledru, P., Johan, V., Milési, J.P. and Tegyey, M. (1994) Markers of the Last Stages of the Palaeoproterozoic Collision: Evidence for a 2 Ga Continent Involving Circum-South Atlantic Provinces. *Precambrian Research*, **69**, 169-191. https://doi.org/10.1016/0301-9268(94)90085-x

[47] Hein, K.A.A., Morel, V., Kagoné, O., Kiemde, F. and Mayes, K. (2004) Birimian Lithological Succession and Structural Evolution in the Goren Segment of the Boromo-Goren Greenstone Belt, Burkina Faso. *Journal of African Earth Sciences*, **39**, 1-23. https://doi.org/10.1016/j.jafrearsci.2004.05.003

[48] John, T., Klemd, R., Hirdes, W. and Loh, G. (1999) The Metamorphic Evolution of the Paleoproterozoic (Birimian) Volcanic Ashanti Belt (Ghana, West Africa). *Precambrian Research*, **98**, 11-30. https://doi.org/10.1016/s0301-9268(99)00024-8

[49] Kříbek, B., Sýkorová, I., Machovič, V. and Laufek, F. (2008) Graphitization of Organic Matter and Fluid-Deposited Graphite in Palaeoproterozoic (Birimian) Black Shales of the Kaya-Goren Greenstone Belt (Burkina Faso, West Africa). *Journal of Metamorphic Geology*, **26**, 937-958. https://doi.org/10.1111/j.1525-1314.2008.00796.x

[50] Liégeois, J.P., Claessens, W., Camara, D. and Klerkx, J. (1991) Short-Lived Eburnian Orogeny in Southern Mali. Geology, Tectonics, U-Pb and Rb-Sr Geochronology. *Precambrian Research*, **50**, 111-136. https://doi.org/10.1016/0301-9268(91)90050-k

[51] Oberthür, T. (1998) Age Constraints on Gold Mineralization and Paleoproterozoic Crustal Evolution in the Ashanti Belt of Southern Ghana. *Precambrian Research*, **89**,

129-143. https://doi.org/10.1016/s0301-9268(97)00075-2

[52] Debat, P., Nikiéma, S., Mercier, A., Lompo, M., Béziat, D., Bourges, F., *et al.* (2003) A New Metamorphic Constraint for the Eburnean Orogeny from Paleoproterozoic Formations of the Man Shield (Aribinda and Tampelga Countries, Burkina Faso). *Precambrian Research*, **123**, 47-65. https://doi.org/10.1016/s0301-9268(03)00046-9

[53] Wenmenga, U. and Affaton, P. (2008) Geochemical Affinity and Geotectonic Setting of Palaeoproterozoic Amphibolites within Granitic-Gneissic Basement of the South Central Area of Burkina Faso, West-Africa. *Global Journal of Geological Sciences*, **6**, 9-22. https://doi.org/10.4314/gjgs.v6i1.18749

[54] Block, S., Jessell, M., Aillères, L., Baratoux, L., Bruguier, O., Zeh, A., *et al.* (2016) Lower Crust Exhumation during Paleoproterozoic (Eburnean) Orogeny, NW Ghana, West African Craton: Interplay of Coeval Contractional Deformation and Extensional Gravitational Collapse. *Precambrian Research*, **274**, 82-109. https://doi.org/10.1016/j.precamres.2015.10.014

[55] Block, S., Ganne, J., Baratoux, L., Zeh, A., Parra-Avila, L.A., Jessell, M., *et al.* (2015) Petrological and Geochronological Constraints on Lower Crust Exhumation during Paleoproterozoic (Eburnean) Orogeny, NW Ghana, West African Craton. *Journal of Metamorphic Geology*, **33**, 463-494. https://doi.org/10.1111/jmg.12129

[56] McFarlane, H.B., Ailleres, L., Betts, P., Ganne, J., Baratoux, L., Jessell, M.W., *et al.* (2019) Episodic Collisional Orogenesis and Lower Crust Exhumation during the Palaeoproterozoic Eburnean Orogeny: Evidence from the Sefwi Greenstone Belt, West African Craton. *Precambrian Research*, **325**, 88-110. https://doi.org/10.1016/j.precamres.2019.02.012

[57] Ganne, J., Gerbault, M. and Block, S. (2014) Thermo-Mechanical Modeling of Lower Crust Exhumation—Constraints from the Metamorphic Record of the Palaeoproterozoic Eburnean Orogeny, West African Craton. *Precambrian Research*, **243**, 88-109. https://doi.org/10.1016/j.precamres.2013.12.016

[58] Blenkinsop, T.G., Oliver, N.H.S., Dirks, P.G.H.M., Nugus, M., Tripp, G. and Sanislav, I. (2020) Chapter 1: Structural Geology Applied to the Evaluation of Hydrothermal Gold Deposits. In: Rowland, J.V. and Rhys, D.A., Eds., *Applied Structural Geology of Ore-Forming Hydrothermal Systems*, Society of Economic Geologists, 1-23. https://doi.org/10.5382/rev.21.01

[59] Markwitz, V., Hein, K.A.A., Jessell, M.W. and Miller, J. (2016) Metallogenic Portfolio of the West Africa Craton. *Ore Geology Reviews*, **78**, 558-563. https://doi.org/10.1016/j.oregeorev.2015.10.024

[60] Masurel, Q., Eglinger, A., Thébaud, N., Allibone, A., André-Mayer, A., McFarlane, H., *et al.* (2021) Paleoproterozoic Gold Events in the Southern West African Craton: Review and Synopsis. *Mineralium Deposita*, **57**, 513-537. https://doi.org/10.1007/s00126-021-01052-5

[61] Baratoux, L., Söderlund, U., Ernst, R.E., de Roever, E., Jessell, M.W., Kamo, S., *et al.* (2018) New U-Pb Baddeleyite Ages of Mafic Dyke Swarms of the West African and Amazonian Cratons: Implication for Their Configuration in Supercontinents through Time. In: Srivastava, R., Ernst, R. and Peng, P., Eds., *Dyke Swarms of the World: A Modern Perspective*, Springer, 263-314. https://doi.org/10.1007/978-981-13-1666-1_7

[62] Tapsoba, B., Lo, C., Wenmenga, U., Iizuka, Y., Chung, S. and Shellnutt, G. (2018) Chemical and Sr-Nd Compositions and $^{40}Ar/^{39}Ar$ Ages of NW-Trending Dolerite Dikes of Burkina Faso: Evidence for a Mesoproterozoic Magmatism in the West African Craton. *Geoscience Frontiers*, **9**, 1957-1980. https://doi.org/10.1016/j.gsf.2017.12.015

[63] Ducellier, J. (1963) Contribution à l'étude des formations cristallines et métamorphiques du Centre et du Nord de la Haute-Volta. Editions Technip, No. 10.

[64] Ganne, J., De Andrade, V., Weinberg, R.F., Vidal, O., Dubacq, B., Kagambega, N., *et al.* (2011) Modern-Style Plate Subduction Preserved in the Palaeoproterozoic West African Craton. *Nature Geoscience*, **5**, 60-65. https://doi.org/10.1038/ngeo1321

[65] Hottin, G. et Ouedraogo, O. (1975) Notice explicative de la carte géologique à 1: 1 000 000 de la république de Haute-Volta. BRGM.

[66] Ilboudo, H. (2010) Le gîte d'amas sulfuré de Tiébélé. Faciès lithologiques, Structures et Minéralisations, Burkina Faso (Afrique de l'Ouest). Ph.D. Thesis, Université de Ouagadougou.

[67] Naba, S. (1999) Structure et mode de mise en place de pluton granitique emboité: Exemple de l'alignement plutonique Tenkodogo-Yamba dans l'Est du Burkina Faso (Afrique de l'Ouest). Ph.D. Thesis, Université Cheikh Anta Diop.

[68] Sagatzky, J. (1950) Notice explicative sur la feuille Tenkodogo Ouest. Gouvernement Général de l'AOF.

[69] Trinquard, R. (1971) Notice explicative de la carte géologique au 1/200.000 de Tenkodogo. BRGM, Archives DGM.

[70] Gaillard, N., Williams-Jones, A.E., Clark, J.R., Salvi, S., Perrouty, S., Linnen, R.L., *et al.* (2020) The Use of Lithogeochemistry in Delineating Hydrothermal Fluid Pathways and Vectoring Towards Gold Mineralization in the Malartic District, Québec. *Ore Geology Reviews*, **120**, Article 103351. https://doi.org/10.1016/j.oregeorev.2020.103351

[71] Gaillard, N., Williams-Jones, A.E., Clark, J.R., Lypaczewski, P., Salvi, S., Perrouty, S., *et al.* (2018) Mica Composition as a Vector to Gold Mineralization: Deciphering Hydrothermal and Metamorphic Effects in the Malartic District, Quebec. *Ore Geology Reviews*, **95**, 789-820. https://doi.org/10.1016/j.oregeorev.2018.02.009

[72] Groves, D.I. (1993) The Crustal Continuum Model for Late-Archaean Lode-Gold Deposits of the Yilgarn Block, Western Australia. *Mineralium Deposita*, **28**, 366-374. https://doi.org/10.1007/bf02431596

[73] Kalinin, A.A., Kazanov, O.V., Kudryashov, N.M., Bakaev, G.F., Petrov, S.V., Elizarov, D.V., *et al.* (2017) New Promising Gold-Ore Objects in the Strelna Greenstone Belt, Kola Peninsula. *Geology of Ore Deposits*, **59**, 453-481. https://doi.org/10.1134/s1075701517060022

[74] Tomkins, A.G., Weinberg, R.F. and McFarlane, C.R.M. (2008) Preferential Magma Extraction from K- and Metal-Enriched Source Regions in the Crust. *Mineralium Deposita*, **44**, 171-181. https://doi.org/10.1007/s00126-008-0204-4

[75] Mériaud, N. and Jébrak, M. (2017) From Intrusion-Related to Orogenic Mineralization: The Wasamac Deposit, Abitibi Greenstone Belt, Canada. *Ore Geology Reviews*, **84**, 289-308. https://doi.org/10.1016/j.oregeorev.2017.01.021

[76] Masurel, Q., Thébaud, N., Allibone, A., André-Mayer, A., Hein, K.A.A., Reisberg, L., *et al.* (2019) Intrusion-Related Affinity and Orogenic Gold Overprint at the Paleoproterozoic Bonikro Au-(Mo) Deposit (Côte d'Ivoire, West African Craton). *Mineralium Deposita*, **57**, 557-580. https://doi.org/10.1007/s00126-019-00888-2

[77] Sangaré, A., Driouch, Y., Salvi, S., Féménias, O., Siebenaller, L., Belkasmi, M. *et al.* (2014) Géologie des minéralisations aurifères du gisement tardi-éburnéen de Kalana (Birimien, Sud-Ouest du Mali) Geology of Kalana late-eburnean gold deposit (Birimian, southwestern Mali). *Bulletin de l'Institut Scientifique*, No. 36, 85-108.

[78] Traoré, Y.D., Siebenaller, L., Salvi, S., Béziat, D. and Bouaré, M.L. (2016) Progressive

Gold Mineralization along the Syama Corridor, Southern Mali (West Africa). *Ore Geology Reviews*, **78**, 586-598. https://doi.org/10.1016/j.oregeorev.2015.11.003

[79] Gauriau, J., Harlaux, M., André-Mayer, A.-S., Eglinger, A., Richard, A., Fontaine, A., *et al.* (2020) Chemical and Boron Isotope Composition of Tourmaline from the Kiaka Orogenic Gold Deposit (Burkina Faso, West African Craton) as a Proxy for Ore-Forming Processes. *Mineralium Deposita*, **57**, 581-600. https://doi.org/10.1007/s00126-020-01002-7

[80] Mathurin, D.B.S., Gbele, O., Allou, G., Barthélémy, K.G. and Inza, C. (2020) Metallotectic Context of the Mineralization of the Tondabo Gold Prospect (Brobo, Center of Côte d'Ivoire, West Africa). *International Journal of Geosciences*, **11**, 325-344. https://doi.org/10.4236/ijg.2020.115017

[81] Lawrence, D.M., Treloar, P.J., Rankin, A.H., Harbidge, P. and Holliday, J. (2013) The Geology and Mineralogy of the Loulo Mining District, Mali, West Africa: Evidence for Two Distinct Styles of Orogenic Gold Mineralization. *Economic Geology*, **108**, 199-227. https://doi.org/10.2113/econgeo.108.2.199

[82] Ridley, J.R. and Diamond, L.W. (2000) Fluid Chemistry of Orogenic Lode Gold Depos-Its and Implications for Genetic Models. In: Hagemann, S.G. and Brown, P.E., Eds., *Gold in* 2000, Society of Economic Geologists, 141-162. https://doi.org/10.5382/Rev.13.04

[83] Eilu, P. and Groves, D.I. (2001) Primary Alteration and Geochemical Dispersion Haloes of Archaean Orogenic Gold Deposits in the Yilgarn Craton: The Pre-Weathering Scenario. *Geochemistry: Exploration, Environment, Analysis*, **1**, 183-200. https://doi.org/10.1144/geochem.1.3.183

[84] Mikucki, E.J. and Ridley, J.R. (1993) The Hydrothermal Fluid of Archæan Lode-Gold Deposits at Different Metamorphic Grades: Compositional Constraints from Ore and Wallrock Alteration Assemblages. *Mineralium Deposita*, **28**, 469-481. https://doi.org/10.1007/bf02431603

[85] Zoheir, B.A. (2008) Characteristics and Genesis of Shear Zone-Related Gold Mineralization in Egypt: A Case Study from the Um El Tuyor Mine, South Eastern Desert. *Ore Geology Reviews*, **34**, 445-470. https://doi.org/10.1016/j.oregeorev.2008.05.003